

# NASA


## MEMORANDUM

Declassified by authority of NASA  
Classification Change Notices No. 209  
Dated \*\* 11-30-70

EXPERIMENTAL INVESTIGATION AT A MACH NUMBER OF 3.11 OF  
THE LIFT, DRAG, AND PITCHING-MOMENT CHARACTERISTICS  
OF A NUMBER OF BLUNT, LOW-FINENESS-RATIO BODIES

By William Letko

Langley Research Center  
Langley Field, Va.

  
**N71-70299**

(ACCESSION NUMBER)

(THRU)

18  
(PAGES)

None  
(CODE)

(NASA CR OR TMX OR AD NUMBER)

(CATEGORY)


**UNCLASSIFIED**

**NASA**  
By Authority of TD-70597 Date 10-19-72

**NATIONAL AERONAUTICS AND  
SPACE ADMINISTRATION**

WASHINGTON

January 1959





## NATIONAL AERONAUTICS AND SPACE ADMINISTRATION

MEMORANDUM 1-18-59L

EXPERIMENTAL INVESTIGATION AT A MACH NUMBER OF 3.11 OF  
THE LIFT, DRAG, AND PITCHING-MOMENT CHARACTERISTICS  
OF A NUMBER OF BLUNT, LOW-FINENESS-RATIO BODIES\*

By William Letko

## SUMMARY

A number of blunt bodies having shapes that may be suitable for atmospheric reentry were tested to determine the lift, drag, and pitching-moment characteristics at a Mach number of 3.11 and a Reynolds number of  $6 \times 10^6$  based on maximum body diameter of 2 inches.


The results of the tests showed that all the bodies were statically stable about a point located one-third of the body length from the nose. The results also showed that high-drag bodies which have a large portion of their afterbodies negatively sloped (decrease in cross-sectional area from nose to base) may have a negative lift-curve slope. This negative slope results from the large negative lift component of the axial force obtained with these bodies and the fact that with negatively sloped afterbodies only small normal forces are developed.

## INTRODUCTION

One of the principal considerations in the design of long-range ballistic missiles is the aerodynamic heating problem. Use of blunt nose shapes appears desirable since they have been shown in reference 1 to have the advantage of low convective heat transfer. Blunt noses have the further advantage that a considerable amount of energy is dissipated through the strong bow wave associated with the blunt shapes.

A further requirement for successful reentry, according to the analysis of reference 2, is that the blunt missile nose must have some margin of dynamic stability along with adequate static stability. The degree of dynamic stability for reentry bodies was shown in reference 2 to be dependent on aerodynamic pitch damping, lift-curve slope, and drag.

\*Title, Unclassified.





The purpose of the present investigation therefore was to provide lift, drag, and static stability data for a number of blunt bodies at a Mach number of 3.11 which could be useful in evaluating the suitability of these shapes for reentry bodies. The characteristics of a pointed  $15^\circ$  cone and the effects of several modifications thereto were also determined.

The aerodynamic characteristics of similar bodies at transonic speeds are presented in reference 3.

### SYMBOLS

The data are referred to the stability system of axes (fig. 1) and are presented in the form of standard coefficients of forces and moments about a point one-third of the length of the model rearward from the front face. The coefficients and symbols used herein are defined as follows:

$C_D$	drag coefficient, $\frac{\text{Drag}}{qS}$
$C_L$	lift coefficient, $\frac{\text{Lift}}{qS}$
$C_m$	pitching-moment coefficient, $\frac{\text{Pitching moment}}{qSd}$
$C_{m_\alpha}$	slope of curve of pitching-moment coefficient with angle of attack, per degree
$C_{m_\delta}$	increment of pitching-moment coefficient per degree of body segment deflection
$C_N$	normal-force coefficient, $\frac{\text{Normal force}}{qS}$
$C_{N_\alpha}$	slope of curve of normal-force coefficient with angle of attack, per degree
$C_{p,b}$	base pressure coefficient
$C_X$	axial-force coefficient, $\frac{\text{Axial force}}{qS}$



D	diameter
d	maximum diameter of model
p	static pressure
q	dynamic pressure, $\frac{\gamma}{2} \rho M^2$
R	radius of curvature
S	maximum cross-sectional area of model
V	free-stream velocity
$\alpha$	angle of attack
$\gamma$	ratio of specific heat at constant pressure to specific heat at constant volume
$\delta$	angle of body segment deflection
$\rho$	mass density of air

#### APPARATUS AND TESTS

The tests were conducted at the Langley gas dynamics laboratory in a blowdown jet having a rectangular test section approximately 12 inches high by 12 inches wide. The nozzle operates at an average Mach number of 3.11. The tests were made at a settling-chamber stagnation pressure of 257 pounds per square inch absolute and the Reynolds number was approximately  $36 \times 10^6$  per foot. For these models, which all had a maximum diameter of 2 inches, the Reynolds number was approximately  $6 \times 10^6$  based on that dimension.

Tests were made through an angle-of-attack range which was different for different models. For some models the range varied from about  $0^\circ$  to  $6^\circ$  and for others the range was from  $0^\circ$  to about  $30^\circ$ . Measurements were made, at each angle of attack, of the normal force, axial force, and pitching moment by means of a sting-supported electrical strain-gage balance.

Base pressures were measured for each model and were used to correct the axial forces measured by the strain-gage balance to the condition of free-stream static pressure acting at the base of the models.

CONFIDENTIAL



The geometric characteristics of the bodies tested are given in figure 2. All models were mounted on an external strain-gage balance which was in turn mounted on a sting. A windshield was provided to protect the balance. All models were made of Duralumin and had a maximum diameter of 2 inches.


## RESULTS AND DISCUSSION

The results of the investigation are presented in figures 3 to 10. The pitching-moment data are presented about a center-of-gravity position which is located one-third of the model length from the nose of each model. The normal and axial forces measured were converted to lift and drag coefficients. Base pressures which were used to correct axial forces to the condition of free-stream static pressure acting on the base of each model are presented in table I.

The lift, drag, and pitching-moment characteristics for models 1 and 2 are shown plotted against angle of attack in figure 3. As can be seen in the figure, the lift-curve slope for both models is negative. This negative lift slope results because bodies with negatively sloped afterbodies (bodies whose cross-sectional area decreases rearward) produce only small normal forces. As a consequence, for blunt high-drag bodies such as models 1 and 2, the negative lift component of the axial force is greater than the lift component of the normal force and results in a negative lift. Model 2, which is the blunter, has the more negative lift-curve slope, and it also has a higher drag than model 1 as would be expected from impact theory because of the flatter face. Both models were stable and had the same static stability.

Models 3 and 4 have positive lift-curve slopes (fig. 4) since they both have fairly high normal forces because of their positive body slope and have axial forces whose negative lift components are not large enough to cancel out the lift components of the normal force. These models also demonstrate that the larger the frontal face area, the greater the drag. Model 4, the blunter of the two models, has the greater drag. The static stability of both models 3 and 4 was about the same near zero angle of attack.

Figure 5 shows that adding a  $15^\circ$  wedge to model 4 (to make model 5), which simulated deflection of a body segment, did not change the slope of the lift or pitching-moment curves appreciably but did provide an increment in lift and pitching moment. A value for  $C_{m\delta}$  of about 0.002 per degree is obtained; however, it appears that only a small trim lift coefficient would result, which would limit the use of such a control for maneuverability. The control, of course, caused a small increase in drag.



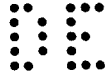


Figure 6 shows the effect on the aerodynamic characteristics of indenting model 4 to form models 6 and 7. Model 6 has the longest flare and, therefore, a shorter portion of the model is negatively sloped. This model has higher lift, a higher stable pitching-moment slope, and slightly higher drag than model 7.

In figure 7 are presented the aerodynamic characteristics of models 8 and 9. Both bodies are the same except for the small cruciform fins on body 9. The negative slope of the bodies and the high axial-force characteristics result in a negative lift-curve slope. The small fins on body 9 have very little effect on the aerodynamic characteristics other than to cause a small decrease in drag. The fins were probably immersed in separated flow and were ineffective in increasing the lift or the stable pitching-moment slopes.

Figure 8 shows the effect on the aerodynamic characteristics of adding a ring to model 10 to form model 11. The purpose of the ring was to fix separation. Both models consisted of a sphere with a portion cut off to form a flat base. The ring increased the slope of the lift curve at low angles of attack, had little effect on the stable pitching moment, and caused a slightly lower drag at low angles and a higher drag at high angles of attack than was obtained with the plain model. A similar result was obtained by adding a ring to model 12 to form model 13 (fig. 9). The flared portion added to the base of the spherical bodies to form models 12 and 13 apparently was in a region of separated flow and had very little effect on the lift and stability. (See figs. 8 and 9.)

Figure 10 shows that rounding the nose or applying a ring to the nose of a  $15^\circ$  cone decreased the lift and pitching-moment slope and had no apparent effect on the drag. Of the bodies tested, the  $15^\circ$  cone and its modifications had the lowest drag, the greatest static stability, and the highest lift-curve slope.

#### COMPARISON OF CALCULATED AND MEASURED

#### AERODYNAMIC CHARACTERISTICS

In table II is presented a comparison between the calculated and experimental values of  $C_{N_\alpha}$ ,  $C_X$  (the axial-force coefficient), and  $C_{m_\alpha}$  for some of the models tested. The calculated values of the derivatives were obtained by use of impact theory as outlined in reference 4.





From the results presented in the table it appears that the most consistent agreement between the measured and calculated values is obtained for  $C_{N\alpha}$ . For  $C_X$  and  $C_{m\alpha}$  the results are inconsistent; for some bodies the agreement is extremely good while for others the calculated values are about 50 percent greater or smaller than the measured values.

#### CONCLUDING REMARKS

The results of an investigation conducted at a Mach number of 3.11 and a Reynolds number of  $6 \times 10^6$ , based on maximum body diameter of 2 inches, to determine the characteristics of a number of blunt bodies showed that all the bodies tested were statically stable about a point located one-third of the body length from the nose. The results also showed that high-drag bodies which have a large proportion of their afterbodies negatively sloped (decrease in a cross-sectional area from nose to base) usually have a negative lift-curve slope. This negative slope results from the large negative lift component of the axial force obtained with these bodies and the fact that with negatively sloped afterbodies only small normal forces are developed.

Langley Research Center,  
National Aeronautics and Space Administration,  
Langley Field, Va., October 7, 1958.

#### REFERENCES

1. Allen, H. Julian, and Eggers, A. J., Jr.: A Study of the Motion and Aerodynamic Heating of Missiles Entering the Earth's Atmosphere at High Supersonic Speeds. NACA TN 4047, 1957. (Supersedes NACA RM A53D28.)
2. Allen, H. Julian: Motion of a Ballistic Missile Angularly Misaligned With the Flight Path Upon Entering the Atmosphere and Its Effect Upon Aerodynamic Heating, Aerodynamic Loads, and Miss Distance. NACA TN 4048, 1957. (Supersedes NACA RM A56F15.)
3. Fisher, Lewis R., Keith, Arvid L., Jr., and DiCamillo, Joseph R.: Aerodynamic Characteristics of Some Families of Blunt Bodies at Transonic Speeds. NASA MEMO 10-28-58L, 1958.
4. Tobak, Murray, and Wehrend, William R.: Stability Derivatives of Cones at Supersonic Speeds. NACA TN 3788, 1956.

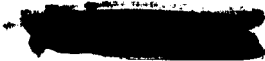




TABLE I.- BASE-PRESSURE-COEFFICIENT DATA FOR MODELS TESTED

$\alpha$ , deg	$C_{p,b}$
Model 1	
0	0.192
2.03	.189
6.10	.189
10.17	.205
14.24	.221
Model 2	
0	0.192
2.03	.192
4.06	.193
Model 3	
0.01	-0.089
2.08	-.084
4.13	-.082
6.20	-.082
10.33	-.083
Model 4	
0	-0.082
2.06	-.081
4.12	-.077
6.17	-.075
10.28	-.074
14.17	-.074
Model 5	
-0.70	-0.089
1.15	-.084
3.31	-.084
5.16	-.084
7.52	-.082
9.59	-.082
11.79	-.082

$\alpha$ , deg	$C_{p,b}$
Model 6	
-0.18	-0.089
1.83	-.089
3.53	-.091
5.74	-.088
7.84	-.089
Model 7	
-0.12	-0.091
1.16	-.089
3.20	-.090
5.29	-.090
7.49	-.091
Model 8	
-1.45	0.201
.76	.201
2.92	.200
4.73	.198
6.44	.200
8.74	.206
10.70	.209
12.36	.211
13.76	.212
15.22	.212
16.57	.212
17.83	.210
19.08	.207
20.49	.207
22.00	.206
23.55	.207
25.00	.209
26.77	.209

$\alpha$ , deg	$C_{p,b}$
Model 9	
-1.20	0.198
.45	.201
2.25	.200
4.01	.195
5.68	.195
7.33	.198
10.04	.205
11.89	.210
13.55	.210
14.95	.210
16.45	.209
18.06	.206
19.62	.207
21.27	.207
22.84	.203
24.26	.203
25.77	.203
27.35	.203
28.97	.195
Model 10	
-0.35	0.188
1.63	.185
3.67	.185
5.45	.190
7.58	.191
9.92	.207
11.95	.217
13.62	.220
15.35	.221
16.92	.221
18.65	.221
20.32	.221
22.16	.211
23.93	.210
26.01	.211
28.05	.209
30.60	.183



CONFIDENTIAL

TABLE I.- BASE-PRESSURE-COEFFICIENT DATA FOR MODELS TESTED - Concluded

$\alpha$ , deg	$C_{p,b}$
Model 11	
-2.14	0.183
-.40	.181
1.64	.170
3.94	.181
5.77	.190
8.17	.190
10.20	.201
12.14	.211
13.97	.215
15.44	.218
17.01	.220
18.54	.220
20.11	.220
21.69	.219
23.16	.214
24.73	.212
26.50	.218
28.33	.211
30.21	.194
Model 12	
-0.50	0.191
1.42	.189
3.71	.185
5.72	.185
8.19	.191
10.42	.203
12.35	.209
13.98	.210
15.80	.212
17.32	.212
18.90	.212
20.58	.211
22.31	.202
24.18	.202
26.01	.203
28.05	.203
30.40	.185

$\alpha$ , deg	$C_{p,b}$
Model 13	
-0.50	-0.189
.98	.189
3.12	.186
5.11	.187
6.85	.188
9.19	.194
11.32	.206
13.25	.212
15.03	.216
17.02	.217
18.13	.217
19.50	.217
21.27	.216
22.84	.215
24.47	.215
27.05	.215
28.17	.212
Model 14	
-2.40	-0.107
-.38	-.107
2.10	-.104
4.80	-.099
7.60	-.099
10.50	-.107
13.65	-.116
Model 15	
-1.30	-0.110
1.30	-.109
3.10	-.107
6.0	-.099
Model 16	
-1.25	-0.104
1.30	-.104
3.90	-.104
6.40	-.099



L-135

TABLE II.- COMPARISON OF CALCULATED AND MEASURED AERODYNAMIC  
COEFFICIENTS FOR SOME OF THE MODELS TESTED

Model	$C_{N_\alpha}$ per deg		$C_X$		$C_{m_\alpha}$ per deg	
	Measured	Calculated	Measured	Calculated	Measured	Calculated
1	0.0120	0.0150	0.77	0.824	-0.0029	-0.0042
2	.0092	.0095	.86	1.28	-.0029	-.0026
3	.0220	.0240	.51	.46	-.0069	-.0108
4	.0200	.0180	.74	.936	-.0067	-.0068
10	.0120	.0175	.73	.67	-.0025	-.0035
14	.0330	.0323	.057	.034	-.0680	-.0460

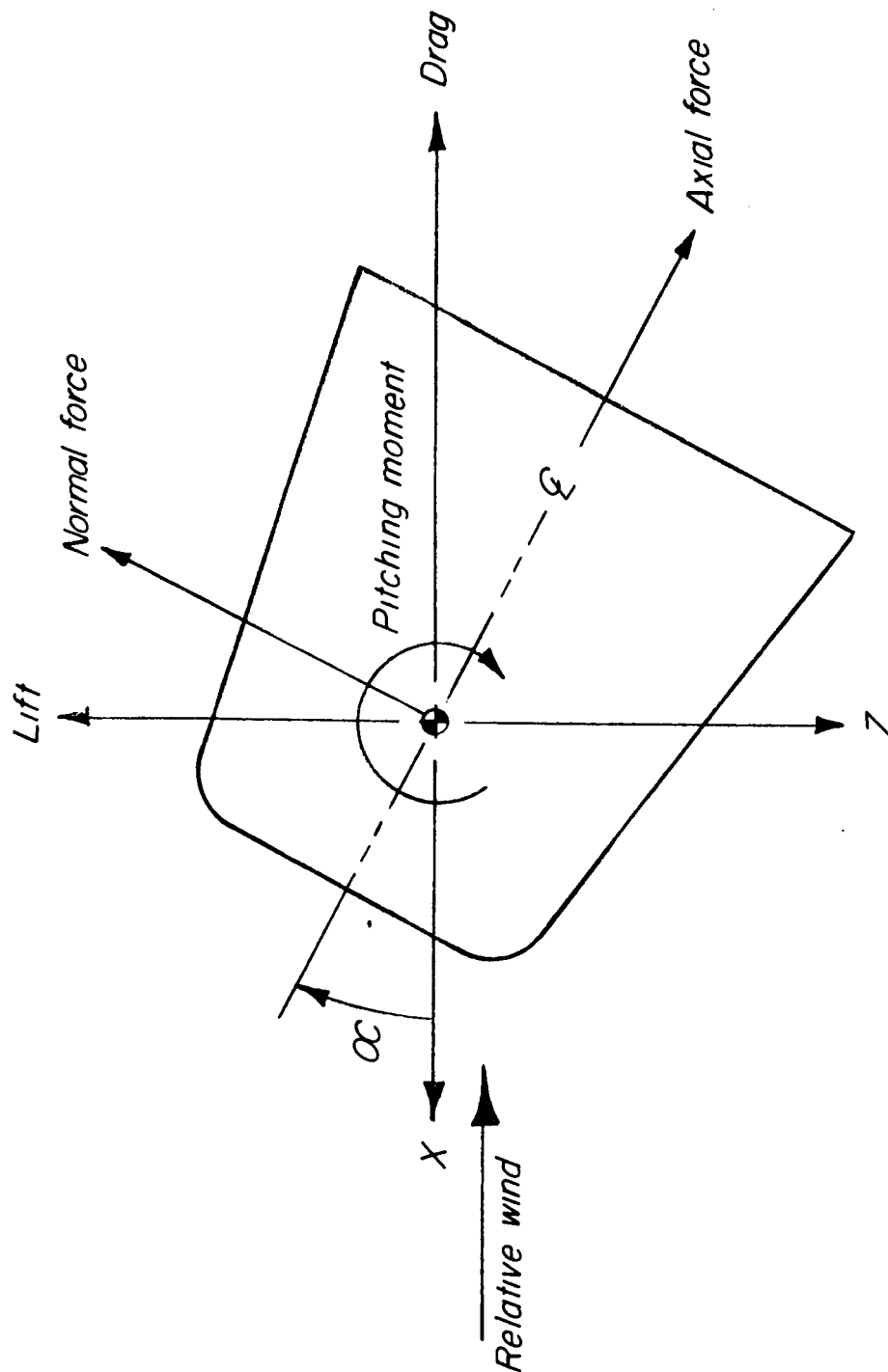
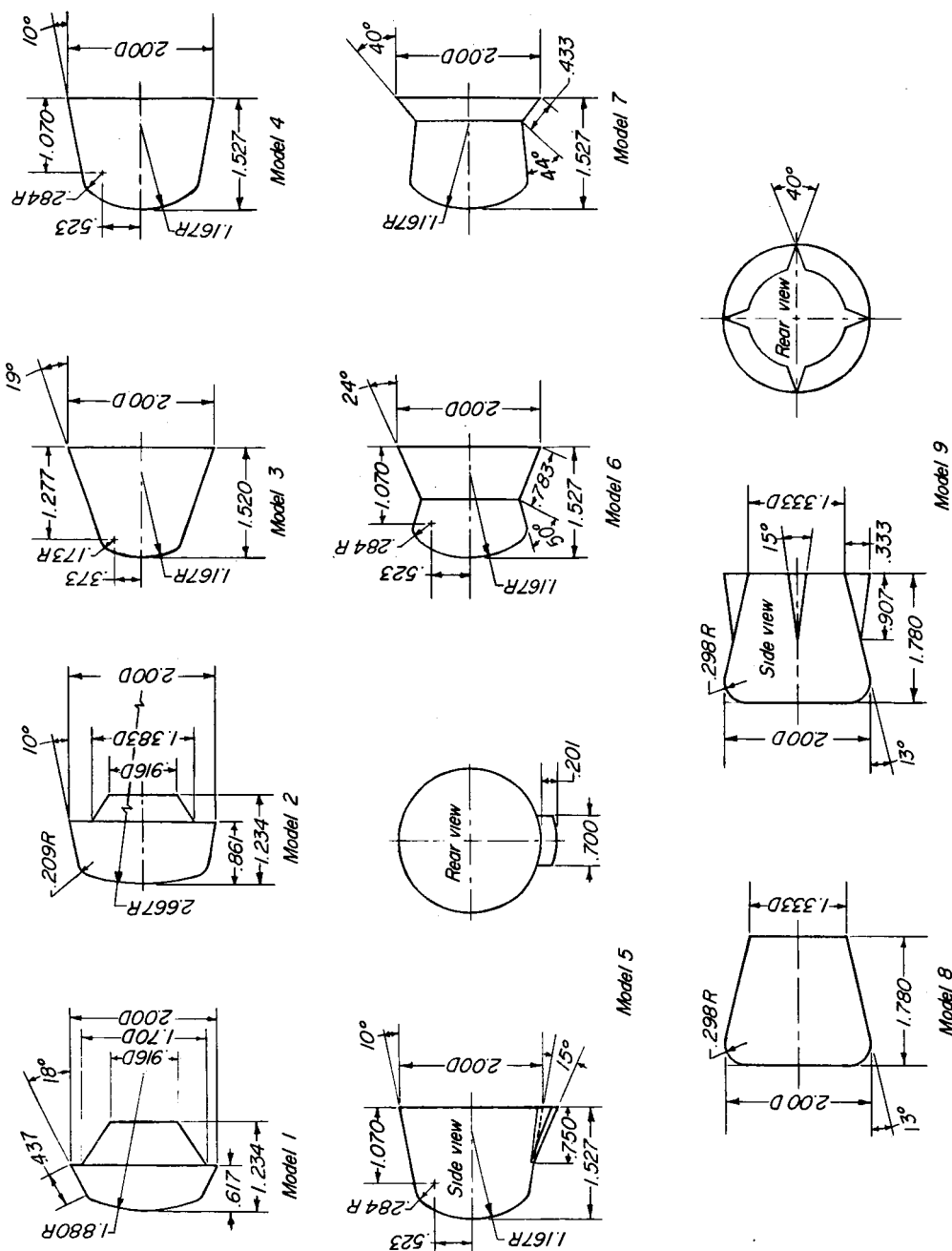
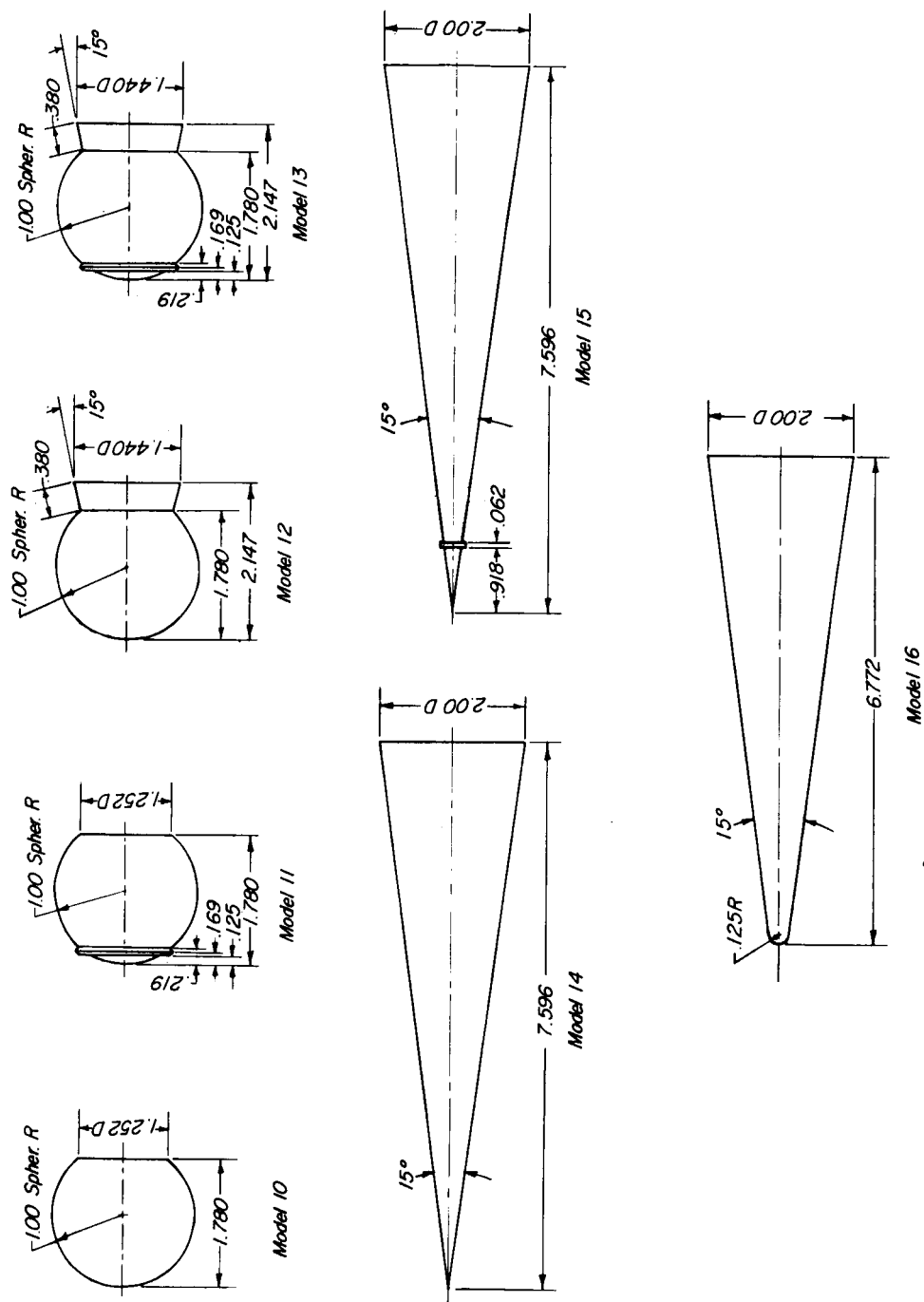


Figure 1.- Stability system of axes. Arrows show positive direction of angles, forces, and moments.



(a) Models 1 to 9.

Figure 2.- Geometric characteristics of models tested.



(b) Models 10 to 16.

Figure 2.- Concluded.

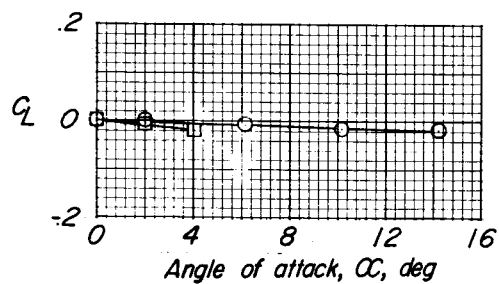
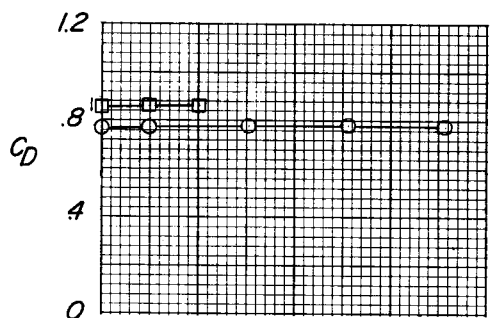
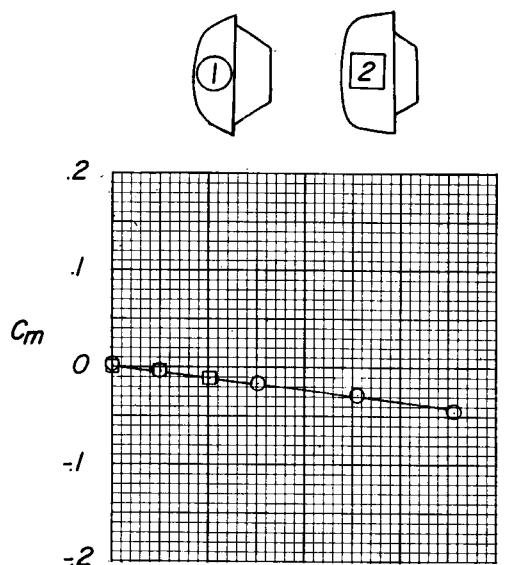


Figure 3.- Aerodynamic characteristics of models 1 and 2.

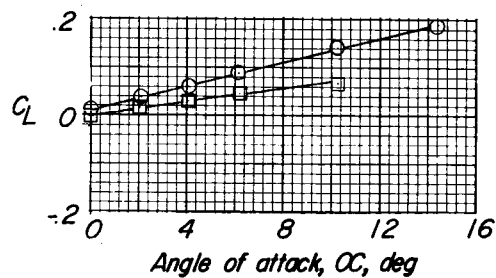
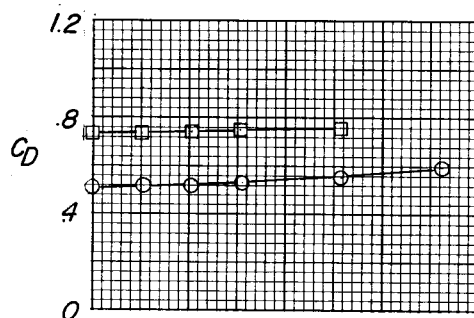
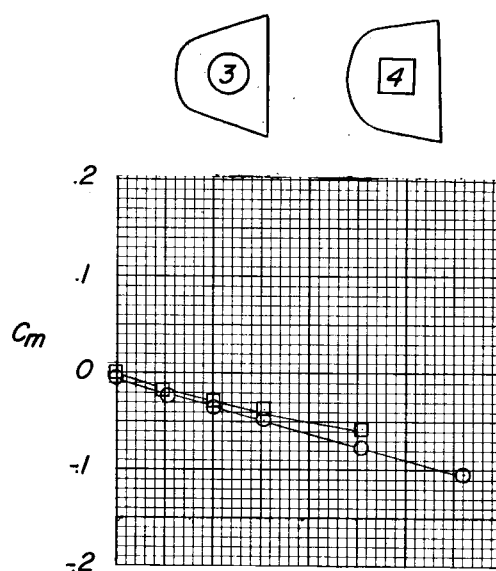
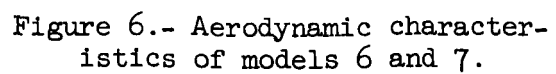
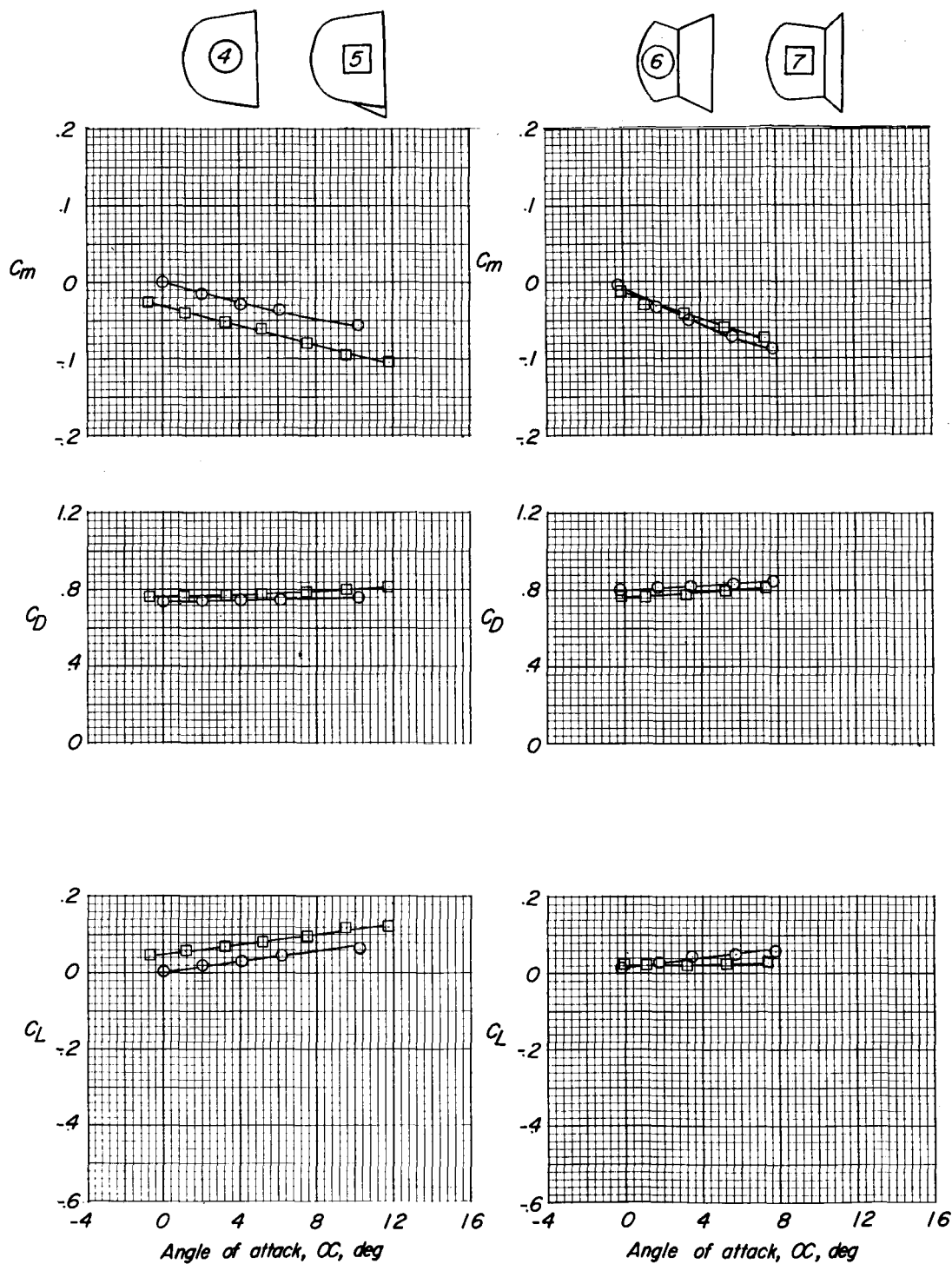


Figure 4.- Aerodynamic characteristics of models 3 and 4.



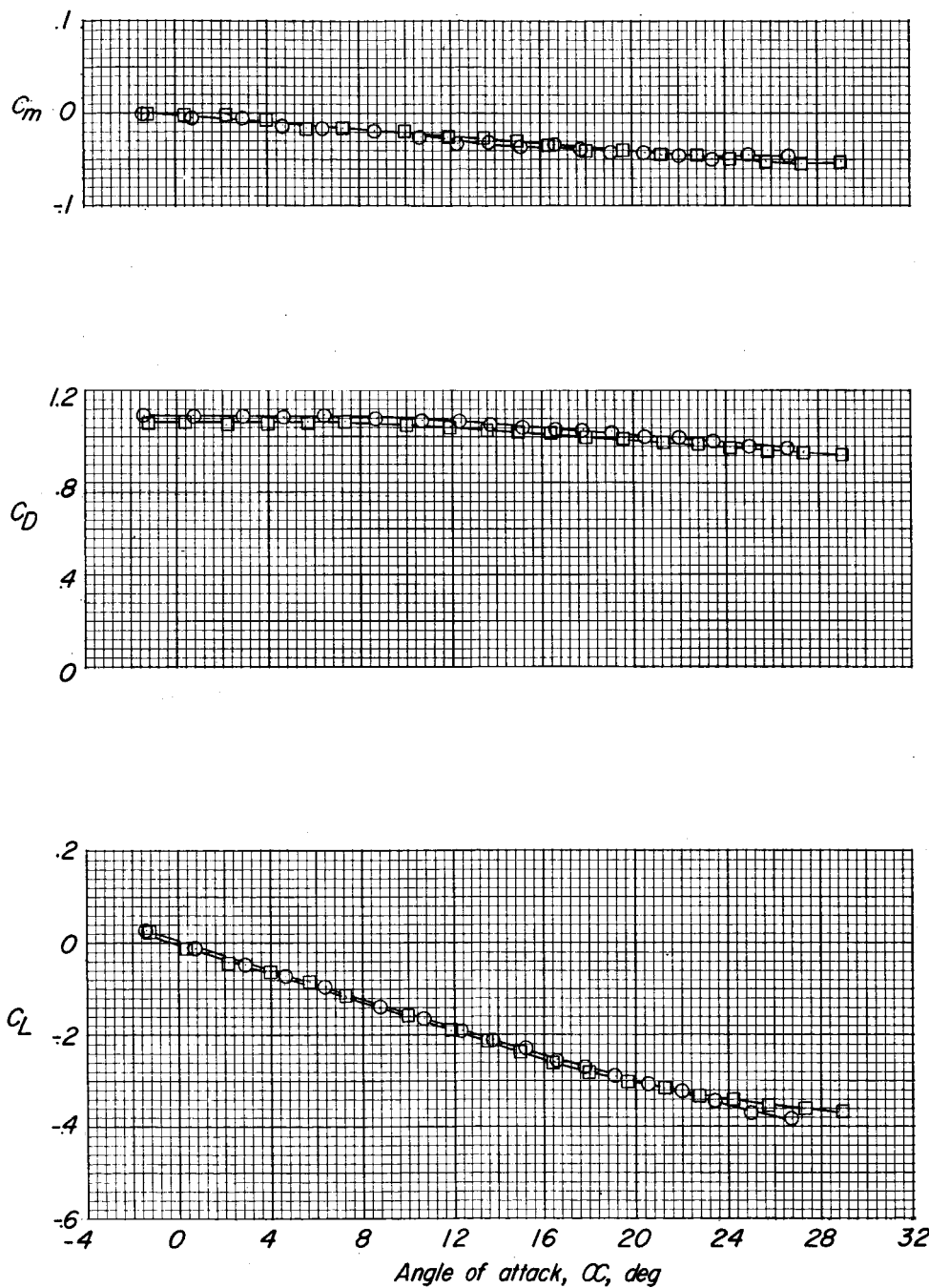
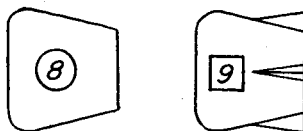


Figure 7.- Aerodynamic characteristics of models 8 and 9.



03712-2-1030

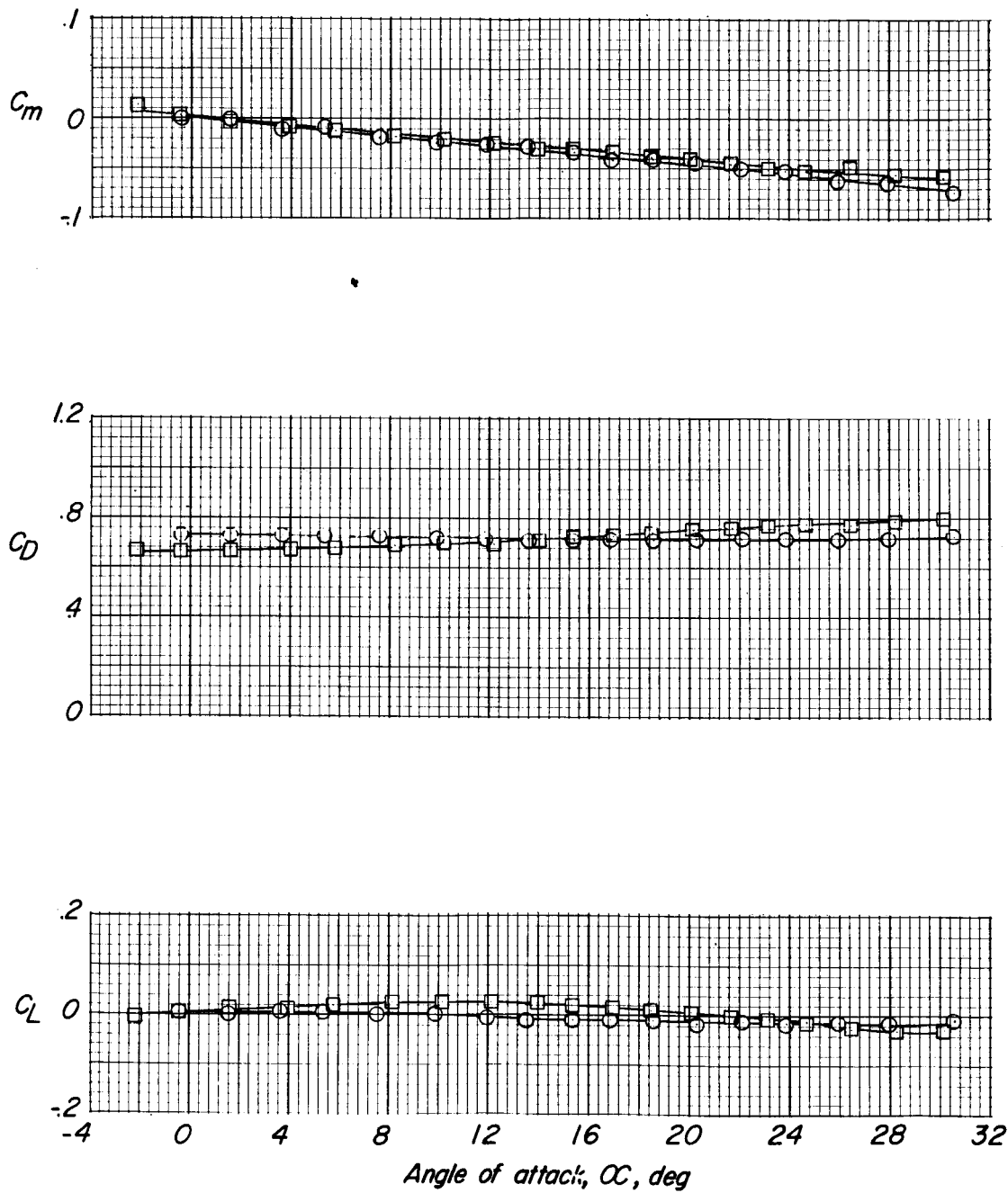
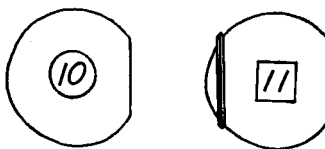


Figure 8.- Aerodynamic characteristics of models 10 and 11.

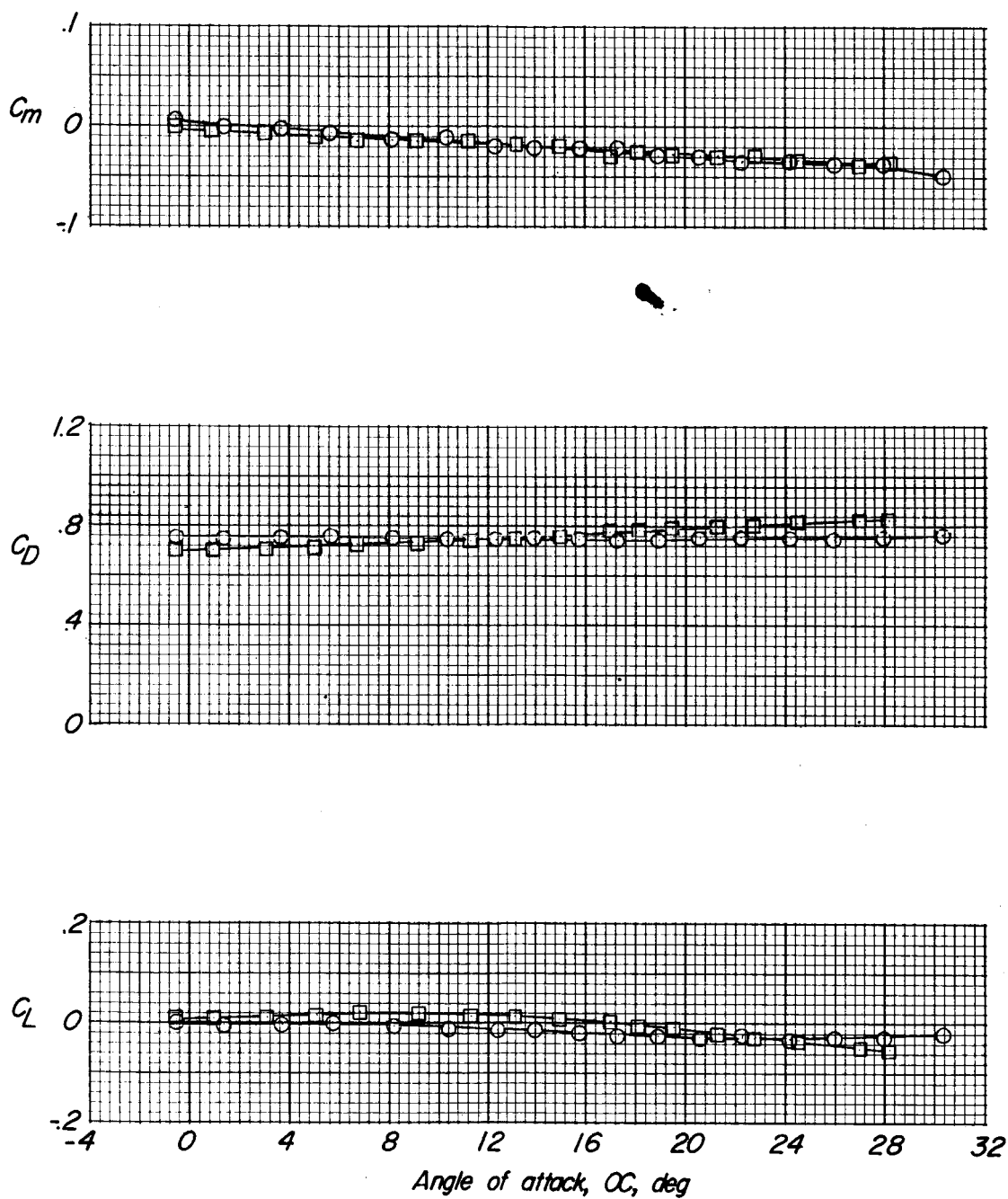
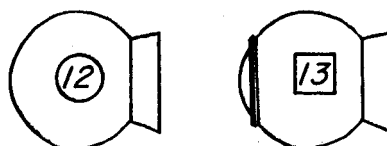


Figure 9.- Aerodynamic characteristics of models 12 and 13.

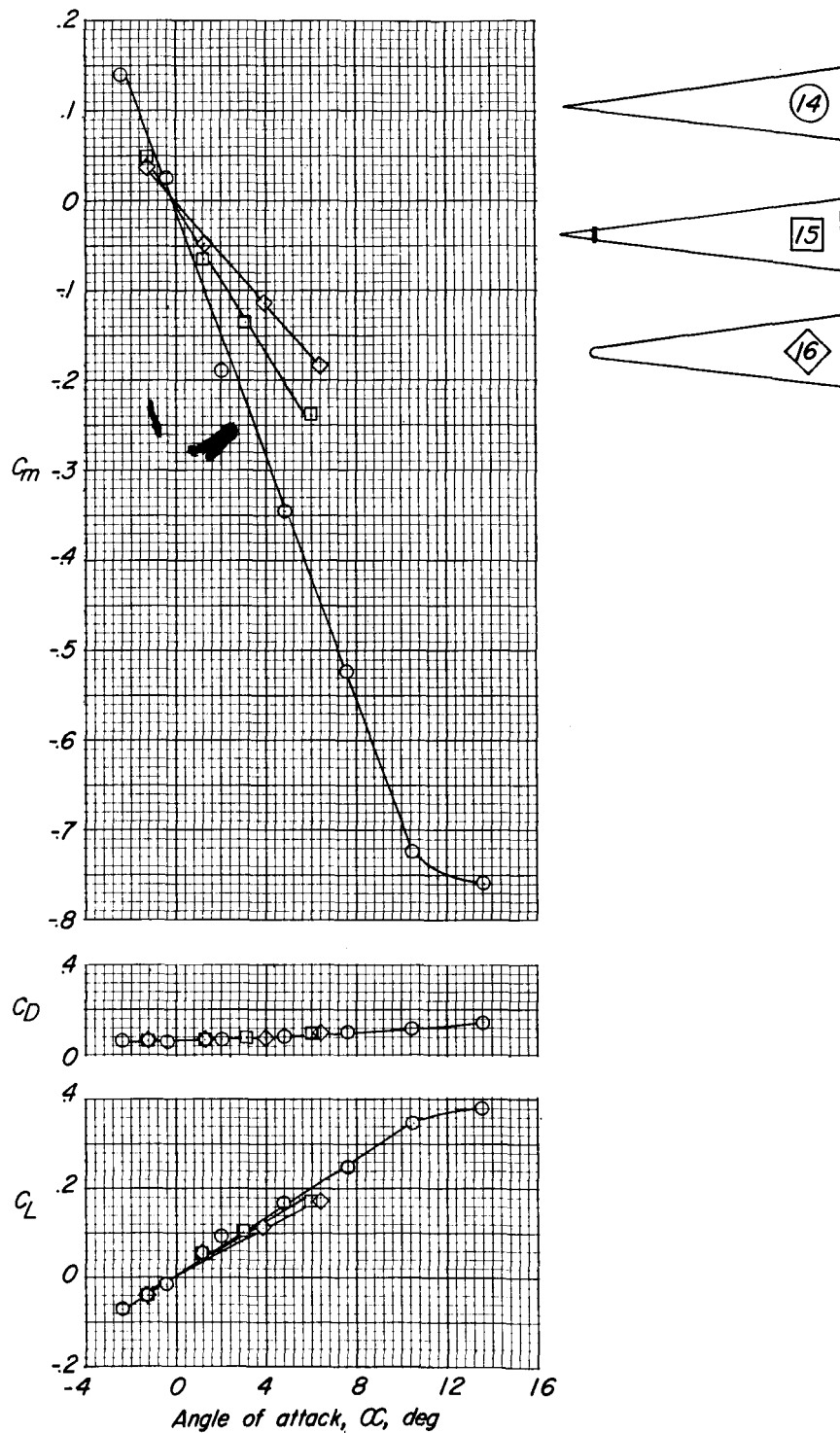


Figure 10.- Aerodynamic characteristics of models 14, 15, and 16.